Melt grafting of sepiolite nanoclay onto poly(3-hydroxybutyrate-co-4-hydroxybutyrate) by reactive extrusion with multi-functional epoxy-based styrene-acrylic oligomer

S. Torres-Giner, N. Montanes, T. Boronat, L. Quiles-Carrillo, R. Balart

Technological Institute of Materials (ITM), Universitat Politècnica de València (UPV), Plaza Ferrándiz y Carbonell 1, 03801 Alcoy, Spain

Corresponding author.
E-mail address: storresginer@hotmail.com (S. Torres-Giner).

Abstract. This paper deals with grafting of sepiolite nanoclay onto poly(3-hydroxybutyrate-co-4hydroxybutyrate) (P(3HB-co-4HB)) biopolymer by melt compounding. Reactive extrusion was performed in a twin-screw extruder in the presence of an epoxy-based styreneacrylic oligomer (ESAO). The chemical interaction of sepiolite with P(3HB-co-4HB) were investigated using Fourier transform infrared (FTIR) spectroscopy. A novel grafting mechanism was proposed based on the multiple epoxy groups present in the reactive coupling agent. Epoxy ring-opening generated, on the one hand, the formation of alkoxy silanes bonds with the silanol groups exposed on the external surface of pristine sepiolite. On the other hand, ester bonds were produced with the terminal acid groups of the biopolymer chains. The newly formed sepiolite-grafted P(3HB-co-4HB) (sepiolite-g-P(3HB-co4HB)) nanocomposite showed higher thermal, thermomechanical, and mechanical performance than the equivalent ungrafted nanocomposite. Melt grafting of sepiolite at different weight contents (1, 3, and 5 wt.-%) interestingly increased the thermal stability and stiffness of P(3HB-co-4HB) without impairing its ductility and toughness.

1. Introduction

Bio-based and biodegradable polymers have received a great deal of attention over the last two decades due to environmental issues. Polyhydroxyalkanoates (PHAs) are a family of biodegradable polyesters that are intracellularly synthesized by microorganisms as carbon and energy reserves. Copolymerization of 3-hydroxybutyrate (3HB) units with of 4-hydroxybutyrate (4HB) units yields to poly(3-hydroxybutyrate-co-4-hydroxybutyrate) (P(3HB-co-4HB)), which represents the latest generation of PHAs [1]. The introduction of 4HB units induces defects in the crystal lattice, making P(3HB-co-4HB) more flexible and less crystalline for practical applications [2]. Different ratios of 3HB vs. 4HB can be achieved depending on the type of microorganism and supplied carbon substrates [3]. This bio-based copolyester can be therefore regarded as a potential candidate to replace polyolefins in packaging applications [4]. Main drawbacks of P(3HB-co-4HB) are related to its poor mechanical strength and low thermal stability, which would restrict its access to the plastics industry when biodegradability is required [5,6].

The incorporation of nanofillers, i.e., fillers below 100 nm, represents a novel solution to promote the industrial use of polymer materials [7]. Due to the ultrathin size of the fillers, polymer nanocomposites can markedly exhibit improved physical properties at low filler contents, i.e., 6 5 in weight (wt.-%) [8]. Up to recent years, the most intensive research was focused on polymer nanocomposites based on plate-like nanoclays, typically montmorillonite (MMT) [9]. However, sepiolite has recently gained increasing consideration because of its particular acicular form, low cost, availability, and extremely high surface area [10]. This nanoclay is a complex hydrated magnesium phyllosilicate ($Mg_4Si_6O_{15}(OH)_26H_2O$). Sepiolite crystals are composed of sheet silicate units that consist of two layers of SiO_4 tetrahedrons in which the unshared oxygen atoms face each other [11]. Tetrahedral layers are bonded with an octahedral layer of coordinated magnesium atoms [12]. This results in a discontinuous longitudinal structure that forms open tunnels, i.e., the so-called ‘‘zeolitic channels”, which run parallel to the axis and present a cross-section of ca. 1.1 0.4 nm^2 [13]. Naturally occurring sepiolite forms bundles of isolated needle-like particles with sizes between 100–5000 nm in length, 10–30 nm in width, and 5–10 nm in thickness [14]. This peculiar structure provides sepiolite with a porous volume of up to 0.4 cm^3/g [15], a surface energy of about 240 mJ/m^2 [16], and a specific surface above 350 m^2/g [17]. Such outstanding properties are responsible for its high sorption capacity and excellent colloidal properties.

Under ambient conditions, $Mg(OH_2)_2$ groups within the channels are completely filled by water [18]. Neither large molecules nor those of low polarity can penetrate the channels and displace the zeolitic water. On the contrary, polar molecules are well absorbed on the external surface of sepiolite, which accounts for 40–50% of its whole surface area [19]. This exposes around 2.2 silanol groups (SiAOH)/100 $Å^2$ [20], which are located every 0.5 nm along the side of the external channels [21]. Silanol groups are easily available for coupling reactions and favor the dispersion of sepiolite in polar matrices [22]. Up to the present, different polymers have been studied for hosting sepiolite such as polypropylene (PP) [10,18,23–27], poly(e-caprolactone) (PCL) [11,28,29], thermoplastic starch (TPS) [12], chitosan [13], poly(ethyl methacrylate) (PEMA) and poly(2-hydroxyethyl methacrylate) (PHEMA) [14], poly(ethylene oxide) (PEO) [17], poly(butylene terephthalate) (PBT) [18], polystyrene (PS) [27], ethylene vinyl acetate (EVA) [27], low-density polyethylene (LDPE) [27,30], linear low-density polyethylene (LLDPE) [31], polyamide 6 (PA 6) [32–35], polyamide 66 (PA 66) [36,37], polyimide (PI) [38], polyurethane (PU) [39–41], epoxy resins [42–44], poly(lactic acid) (PLA) [28,29,45–49], poly(butylene adipate-co-terephthalate) (PBAT) [50], poly(hydroxyethyl acrylate) (PHEA) [51], gelatin [52,53], poly(vinyl alcohol) (PVA) [54], and poly(sodium acrylate) (PSA) [55]. Additionally, sepiolite has been proposed to compatibilize immiscible polymer blends such as bio-based high-density polyethylene (bio-HDPE)/TPS [22], LDPE/TPS [56], LDPE/PLA [57], PLA/PP [58], and TPS/PBAT [59]. Most of these previous works have showed that the introduction of sepiolite habitually leads to a mechanical and thermal improvement due to the high aspect ratio of the nanoclay. Additionally, other materials properties can be improved such as rheology [25,56], biocompatibility [47,50], biodegradation [29], and flame retardancy [25,26,45]. Sepiolite can also enlarge the

operating window of a given polymer, which certainly results advantageous for P(3HB-co-4HB) in the replacement of commodity plastics [24].

Effective reinforcement is related, however, to a good dispersion of the nanoclay within the polymer matrix. This can be only achieved when non-trivial prerequisites (e.g., good nanofiller dispersion, orientation, and positive matrix-filler interactions) are fulfilled. Unfortunately, sepiolite, similar to other nanoclays, is habitually aggregated in nature and physical mixing can hardly provide desired dispersion at the nanometer scale. To attain effective disaggregation, diverse organic modifications can be applied on the sepiolite surface. These mainly include hydrophobic silanes such as 3aminopropyl triethoxyl silane (3-APTS) [14], propyltrimethoxy silane (PTMS) [22], octyl trimethoxy silane (OTMS) [30], and vinyl triethoxy silane (VTES) [31]. Some authors have also employed other chemical treatments, for instance polyethylene glycol (PEG) [17], quaternary ammonium salts [18], cethyl trymethyl ammonium bromide (CTAB) [25,26], dimethyl benzyl hydrogenated tallow quaternary ammonium (B2MTH) [35], trimethyl hydrogenated tallow quaternary ammonium (3MTH) [32,35], and N-hydrogenated tallow-1,3-diaminopropane (DIAMIN T) [35]. Nevertheless, their application adds complexity and increases the manufacturing costs of the final polymer nanocomposite. Moreover, certain poor thermal stability can be induced, especially when used in combination with polymers that need to be processed at high temperatures.

The large concentration of silanol groups on sepiolite offers high functionality, which therefore opens up new coupling reactions with polar matrices. In particular, SiAOH can react with epoxides in vapor phase. This reaction opens the epoxy rings followed by combination with the resulting organic species on the silicate surface [60]. In the field of polymer science, bi-functional and multi-functional epoxy-based oligomers are currently used as ‘‘chain extenders”. These are mainly applied for polyesters, recently including PHAs [61]. The use of the so-called chain extenders basically leads to an increase in the polymer molecular weight (M_W), which in turn improves melt strength and thermal stability. These have also been recently reported to perform as compatibilizer in blends of polyesters [62]. At high temperatures, the epoxy functions trigger the formation of covalent bonds with both nucleophilic terminal groups of polyesters chains, i.e., hydroxyl (AOH) and carboxyl (ACOOH) groups [63]. This paper describes the first attempt to graft pristine sepiolite onto P(3HB-co-4HB) biopolymer by reactive extrusion using a functional coupling agent containing multiple epoxy groups.

2. Materials and methods

2.1. Materials

Bacterial aliphatic copolyester P(3HB-co-4HB) was Mirel P1004, supplied by Metabolix, Inc. (Woburn, USA). This is a home-compostable grade up to 488 lm designed for injection molding. The resin presents a M_W of 2.9 10^5 g/mol, with a polydispersitivity index (PDI) of 1.62, a melt flow rate of 14 g/10 min (190 C/2.16 kg), and a density of 1.3 g/cm^3. The molar fraction of 4HB in the copolymer is approximately 5%. Unmodified sepiolite was kindly supplied by Grupo Tolsa S.A. (Madrid, Spain) under the trade name of Pansil 400. The nanoclay is obtained from the Tagus river basin and the bulk density of the powder is 60 ± 30 g/L. Joncryl ADR 4368-C was provided by BASF S.A. (Barcelona, Spain) in the form of solid flakes. This is a proprietary epoxy-based styrene-acrylic oligomer (ESAO) with number average functionality (f) > 4. Styrene and acrylic building blocks are each between 1 and 20. M_W is 6800 g/mol, glass transition temperature (T_g) is 54 C, and the epoxy equivalent weight (EE_W) is 285 g/mol. Recommended dosage by manufacturer is 0.1–1 wt.-% for appropriate processability of biodegradable polyesters.

2.2. Reactive extrusion

Prior to processing, to remove residual moisture, the P(3HB-co-4HB) pellets and sepiolite powder were stored at 60 C for 36 h in a dehumidifying dryer MD from Industrial Marsé (Barcelona, Spain). P(3HB-co-4HB) and sepiolite were compounded in a co-rotating ZSK-18 MEGAlab laboratory twin-screw extruder from Coperion (Stuttgart,

Germany). The screws feature 18 mm diameter with a length (L) to diameter (D) ratio, i.e., L/D, of 48. The barrel is divided into 11 segments, including the strand die head. P(3HB-co-4HB) pellets were fed into the main hopper while sepiolite and ESAO were introduced through a ZS-B 18 twin-screw side feeder from K-Tron (Pitman, USA), located at segment number 4. Materials dosage was set to achieve a residence time of about 1 min. The screws speed was fixed at 300 rpm. The extrusion temperature profile, from the hopper to the die, was set as follow: 165–170–170–175–175–180–180 C. The strand was cooled in a water bath and then pelletized using an air-knife unit. Table 1 summarizes the different samples prepared during the melt compounding.

2.3. Injection molding

P(3HB-co-4HB)/sepiolite nanocomposites were shaped for characterization using an injection-molding machine 270/75 from Mateu & Solé (Barcelona, Spain). The profile temperature, from the feeding zone to the injection nozzle, was set as follows: 155–160–165–170 C. A clamping force of 75 tons was applied. The cavity filling and cooling time were set at 1 and 10 s, respectively. Standard samples with a thickness of 4 mm were obtained and stored at room conditions, i.e., 23 C and 50% HR, for 15 days before characterization.

2.4. Morphology

Morphologies of the sepiolite powder and the fractured surfaces of the P(3HB-co-4HB) nanocomposites were observed by scanning electron microscope (SEM) with a Zeiss Ultra 55 from Oxford Instruments (Abingdon, UK). An acceleration voltage of 2 kV was applied. Surfaces were previously coated with a gold-palladium alloy in a sputter coater EMITECH model SC7620 from Quorum Technologies, Ltd. (East Sussex, UK). Detailed morphology of sepiolite was obtained by transmission electron microscopy (TEM) with a JEM-2010 microscope from JEOL (Tokyo, Japan) using an acceleration voltage of 100 kV. This was equipped with an ORIUSTM SC600 TEM CCD camera for image acquisition. Sepiolite sizes were measured using Image J software.

Table 1
Samples prepared according to the content of poly(3-hydroxybutyrate-co-4-hydroxybutyrate) (P(3HB-co-4HB)), epoxy-based styrene-acrylic oligomer (ESAO), and sepiolite nanoclay.

Samples	Percentage (wt.-%)		
	P(3HB-co-4HB)	ESAO	Sepiolite
P(3HB-co-4HB)	100	0	0
P(3HB-co-4HB) + ESAO	99	1	0
P(3HB-co-4HB) + Sepiolite 1 wt.-%	99	0	1
P(3HB-co-4HB) + ESAO + Sepiolite 1 wt.-%	98	1	1
P(3HB-co-4HB) + ESAO + Sepiolite 3 wt.-%	96	1	3
P(3HB-co-4HB) + ESAO + Sepiolite 5 wt.-%	94	1	5

2.5. Infrared spectroscopy

Chemical analyses was performed using attenuated total reflection–Fourier transform infrared (ATR-FTIR) spectroscopy. Spectra were recorded with a Vector 22 from Bruker S.A. (Madrid, Spain) coupling a PIKE MIRacle™ ATR accessory from PIKE Technologies (Madison, USA). Ten scans were averaged from 4000 to 400 cm^{1} at a resolution of 4 cm^{1}.

2.6. Thermal analysis

Crystallization and melting behavior of P(3HB-co-4HB) and its nanocomposites were conducted in a differential scanning calorimetry (DSC) 821 model from Mettler-Toledo, Inc. (Schwerzenbach, Switzerland). For this,

approximately 5 mg of sample was placed in 40-ll hermetic aluminum sealed pans, previously calibrated with an indium standard. The analysis was performed in a dry reducing atmosphere in which nitrogen flowed at a constant rate of 66 mL/min. Samples were subjected to a three-step program at a heating rate of 10 C/min. An initial heating cycle from 30 to 200 C was applied to remove the thermal history, followed by a cooling to 50 C, and a final increase to 350 C to evaluate the thermal transitions. The crystallization temperature from the melt (T_c) and enthalpy of crystallization (DH_c) were obtained from the first cooling scan while the melting temperature (T_m), enthalpy of melting (DH_m), and cold crystallization (DH_{cc}) were determined from the second heating scan. The percentage of crystallinity (X_c) was obtained by the following equation:

$$Xc = \left[\frac{\Delta Hm - \Delta Hcc}{\Delta H_m^0 \cdot (1 - w)}\right] \cdot 100$$

where DH^0_m ¼ 146 J/g is the theoretical enthalpy corresponding to the melting of a 100% pure crystalline sample of poly(3-hydroxybutyrate) (PHB) [64] and w represents the filler weight fraction.

Thermogravimetric analysis (TGA) was used to evaluate the thermal stability of P(3HB-co-4HB) and its nanocomposites in a TGA/SDTA 851 thermobalance from Mettler Toledo, Inc. (Schwerzenbach, Switzerland). The heating program was set from 30 to 700 C at a heating rate of 20 C/min in nitrogen with a constant flow rate of 66 mL/min. Approximately 10 mg of each sample was used for the measurements. The onset degradation temperature was defined as the temperature at 5% weight loss ($T_{5\%}$) and the degradation temperature (T_{deg}) was obtained from the maximum value of the first derivative peak.

2.7. Thermomechanical characterization

Dynamic mechanical thermal analysis (DMTA) was performed using an AR-G2 device from TA Instruments (New Castle, USA) equipped with a torsion clamp system in torsion-shear mode. To determine the storage modulus (G_0), loss storage modulus (G_{00}), and loss tangent (tan d), samples were scanned from 60 to 100 C at a heating rate of 2 C/min, a frequency of 1 Hz, and a strain amplitude (c) of 0.1%. The dimensions of the tested samples were 4 10 40 mm^3. All measurements were done in triplicate.

2.8. Mechanical tests

Injection-molded specimens with a dumbbell shape, a total length of 150 mm, and a cross-section of 10 4 mm^2 were tested in a universal test machine ELIB 30 from S.A.E. Ibertest (Madrid, Spain). Tensile and flexural tests were performed according to ISO 527 and 178, respectively. In both tests a 5 kN load cell and a cross-head speed of 5 mm/min were employed. Shore D hardness was determined in a durometer 676-D model from J. Bot S.A. (Barcelona, Spain) following ISO 868. Impact strength was tested in a 1-J Charpy pendulum from Metrotec S.A. (San Sebastián, Spain), as suggested by ISO 179. All specimens were tested in a controlled chamber at room conditions, i.e., 23 C and 50% RH. Six samples for each material were analyzed and averaged.

3. Results

3.1. Morphology of nanoclay

Fig. 1a shows a SEM micrograph of the sepiolite powder. The image basically revealed the characteristic fiber-like structure of sepiolite, which was mainly presented as bundle-like aggregates of nano-sized needles. These micrometric assemblies are naturally produced because of the high surface interaction between individual nanoparticles [32]. To better ascertain the nanoclay morphology, TEM characterization was performed. As shown in Fig. 1b, sepiolite

morphology was certainly based on a needle-shaped nanostructure with dissimilar sizes. In the TEM image, it can be observed that the large needles observed by SEM were actually formed by the presence of discontinuous shorter nanoparticles. Isolated nanoparticles also showed the typical tubular structure of sepiolite, which leads to its highly porous morphology. These tunnels, as previously indicated, are formed as a consequence of alternating tetrahedral-octahedral-tetrahedral plates along the longitudinal axis of the nanoclay.

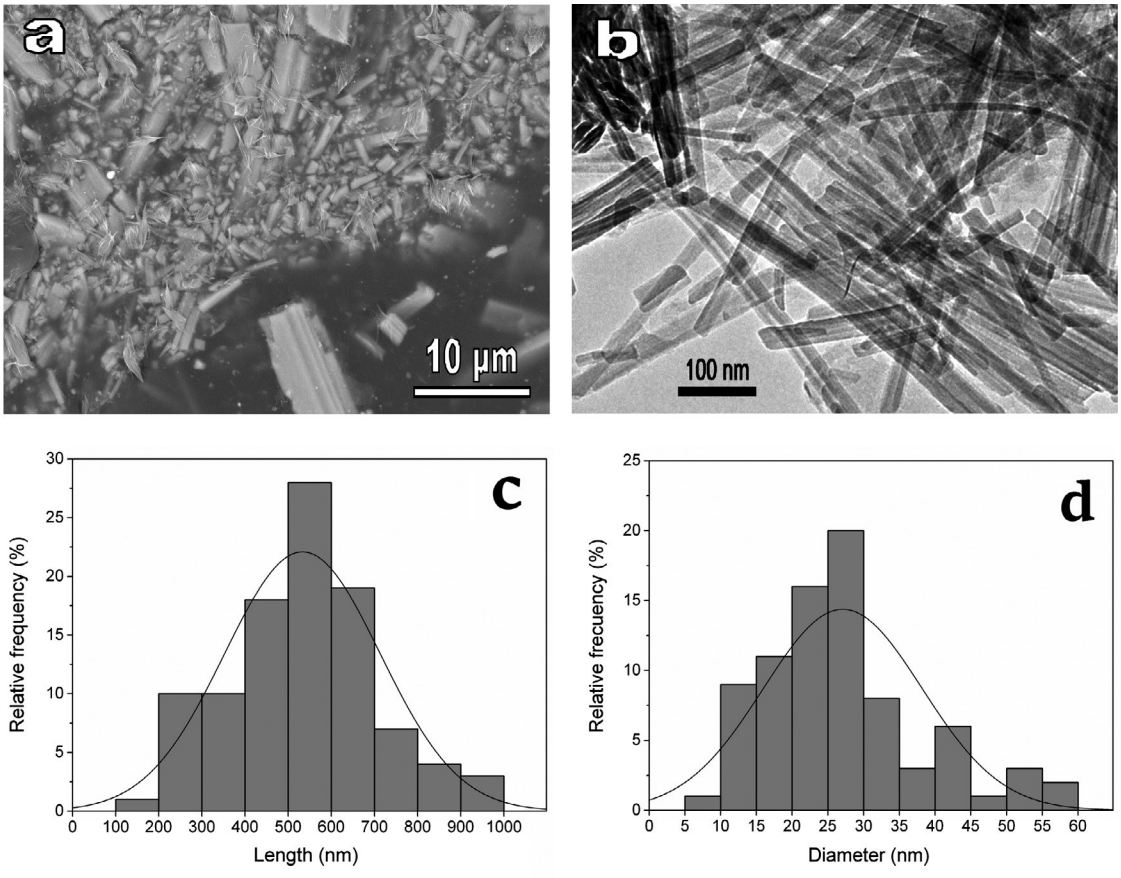

Fig. 1. (a) Scanning electron microscope (SEM) image of sepiolite powder. Scale marker of 10 lm; (b) Transmission electron microscopy (TEM) image of sepiolite powder. Scale marker of 100 nm; (c) Histogram of sepiolite length (L); (d) Histogram of sepiolite diameter (D).

The histograms of the nanoparticle length (L) and diameter (D) of sepiolite are shown in Fig. 1c and d. Mean values of L and D were ca. 540 and 27 nm, respectively. The aspect ratio, i.e., L/D, was determined at 20, which is a positive geometric indicator for mechanical reinforcement in polymer matrices. In this sense, there is a positive correlation between the mechanical properties and the aspect ratio in fiber-reinforced nanocomposites: The higher the aspect ratio, the higher the tensile strength [65]. High values of L/D are therefore habitually needed for achieving optimal reinforcement. The observed aspect ratio of sepiolite is in agreement with Sabzi et al. [46], who reported values of L of 7 lm and D of 340 nm for Turkish sepiolite, i.e., a mean L/D of 21. The average sizes of sepiolite nanoclay have been described elsewhere, showing values in the range of 1000–2000 nm for L and 20–30 nm for D [23,32,39].

3.2. Structural analysis

ATR-FTIR was performed to evaluate chemical interactions between P(3HB-co-4HB), sepiolite, and ESAO. FTIR spectra of the sepiolite powder, ESAO flakes, neat P(3HB-co-4HB), and its nanocomposites are gathered in Fig. 2a. In relation to the nanoclay, the spectrum of the pristine sepiolite powder showed a broad intensity in the region from 1100 to 900 cm^{1}. Main peaks were particularly seen at 1008 and 976 cm^{1}, which have been respectively identified as

the SiAO ‘‘cage-like” and ‘‘network” stretching modes [31,66]. The main peak for the CAO stretching vibration of the epoxy groups in the spectrum of ESAO appeared around 1180, 910, 850, and 760 cm^{1} [67–69]. In the P(3HB-co-4HB)-based materials containing ESAO these peaks disappeared, indicating that these functional groups reacted and were consumed during the meltcompounding process. For the biopolymer, the stretching vibration of the carbonyl group (C@O) produced a strong and sharp peak at ca. 1724 cm^{1} that corresponds to the intramolecular bonding of the crystalline state of P(3HB-co-4HB) [70,71]. The stretching bands of the carbon–carbon single bond (CAC) also gave rise to complex and multiple peaks in the region from 1000 to 880 cm^{1}, containing a sharp and intense band centered around 978 cm^{1} [72].

Fig. 2b shows the spectra details for both P(3HB-co-4HB) nanocomposites containing 1 wt.-% of sepiolite prepared with and without ESAO. Arrows indicate the identified chemical groups formed in the spectra. By comparison of both spectra, it can be seen that the strongest band in the P(3HB-co-4HB) spectrum, which corresponds to the crystalline C@O stretching

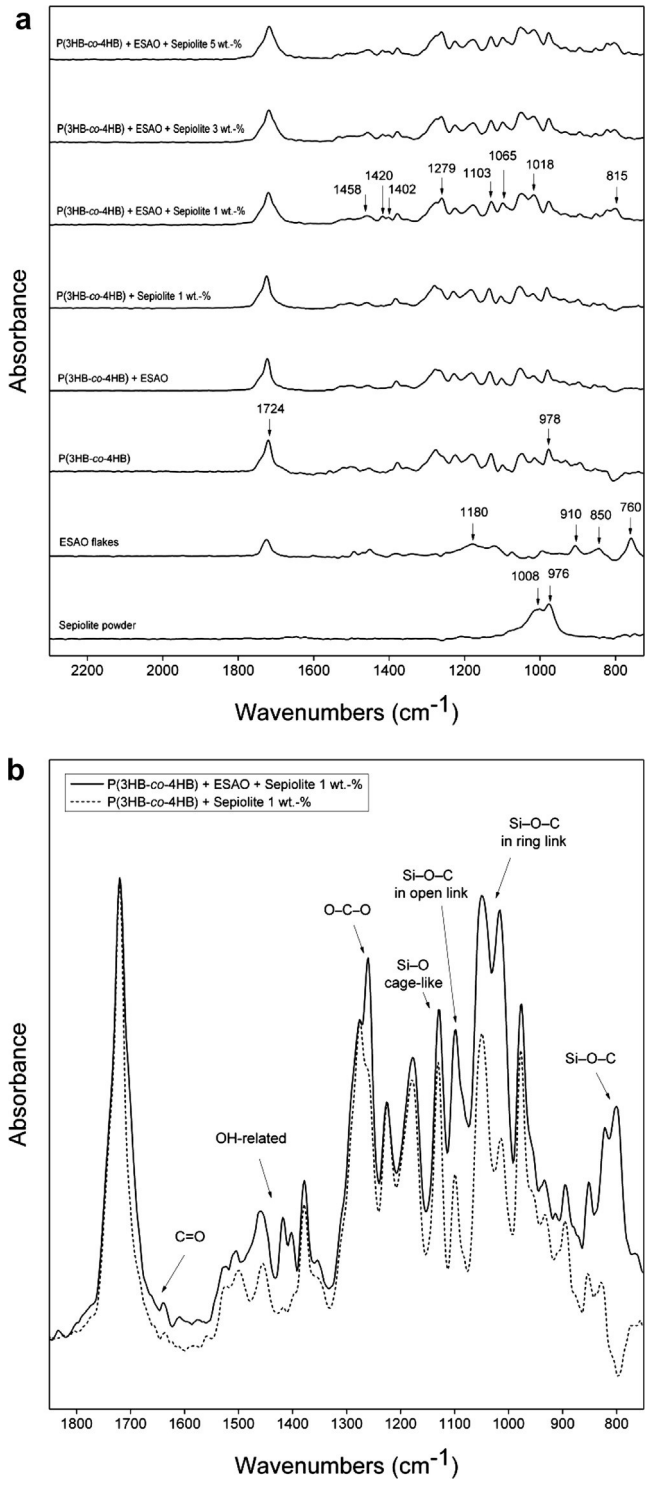

Fig. 2. (a) Fourier transform infrared (FTIR) spectra, from bottom to top, of: Sepiolite powder, epoxy-based styrene-acrylic oligomer (ESAO) flakes, poly(3hydroxybutyrate-co-4-hydroxybutyrate) (P(3HB-co-4HB)), P(3HB-co-4HB) with ESAO, P(3HB-co-4HB) with sepiolite at 1 wt.-%, P(3HB-co-4HB) with ESAO and sepiolite at 1, 3, and 5 wt.-%. Arrows indicate the wavenumbers of the bands described in the text; (b) Detail of the FTIR spectra for the ungrafted and melt-grafted P(3HB-co-4HB)/sepiolite 1 wt.-% nanocomposites. Arrows indicate the chemical bonds described in the text.

vibration, was kept at 1724 cm^{1}. Interestingly, combination of ESAO with sepiolite broadened the carbonyl peak and generated a shoulder at approximately 1705 cm^{1}. This indicates that the hydrogen bonding in the molecular arrangement of P(3HB-co-4HB) was altered, which could be produced due to an intramolecular disruption of the biopolymer chains by the presence of sepiolite. Some authors have also ascribed shifts in this peak to the reaction between the epoxy groups of the chain extender and the carboxyl groups (ACOO) in polyesters [73]. Additionally, an intensity increase in the AOACAOA stretching vibration peak, related to the carboxyl group at 1279 cm^{1} [71], also proved the formation of new ester groups. The intense bonding mode observed at ca. 1150 cm^{1} is for the SiAO cage-like stretching mode [66]. Interaction of the nanoclay with the P(3HB-co-4HB) matrix was also supported by the intensity increase in the band centered at 1103 cm^{1} and both major bands at ca. 1065 and 1018 cm^{1} that correspond to the SiAOAC bands in their ‘‘open” and ‘‘ring” links, respectively [74]. The presence of this new SiAOAC bond was further evidenced by the strong signal near 815 cm^{1} [74]. Interestingly, the spectra of the P(3HB-co-4HB) nanocomposite produced with ESAO also showed a new group of bands at 1420– 1500 cm^{1}, with main intensities at ca. 1402, 1420, and 1459 cm^{1}. These bands are ascribed to the CAH bending in close proximity to the newly formed OH-related bonds during the hydroxyl side group formation [74,75]. These peaks were not observed in the spectrum of the P(3HB-co-4HB)/sepiolite nanocomposite prepared without ESAO, which confirmed the chemical bonding of sepiolite to the biopolymer.

The above results clearly indicate that intramolecular changes took place in the P(3HB-co-4HB) structure. More importantly, the presence of new bands related to SiAOAC bonds supports the fact that covalent bonds were formed between the biopolymer and the reactive SiAOH groups of sepiolite. This chemical interaction could be intensified due to the high surface area of sepiolite. Based on the above FTIR results, Fig. 3 suggests the possible grafting mechanism of sepiolite onto the biopolymer during reactive extrusion. On one hand, in the case of the biopolymer, ester bonds are formed by the reaction of terminal acid groups of P(3HB-co-4HB) with the epoxy functional groups of ESAO. The mechanisms of epoxy-based chain extension in polyesters by these highly reactive compounds have been long discussed in the literature [63]. This mainly consists on glycidyl esterification of carboxylic acid end groups, which precedes hydroxyl end group etherification. This latter reaction competes with etherification of secondary hydroxyl groups and main chain transesterification. In this sense, it has been reported that the reaction rate of the epoxide in polyesters is about 10–15 times higher with the carboxyl (ACOO) than the hydroxyl (AOH) group [76]. On the other hand, an alkoxy carbonyl silane structure is proposed to take place through the reaction of the external SiAOH groups of sepiolite with other epoxy groups present in the acrylic units of ESAO. This reaction involves epoxy ring-opening and the creation of covalent SiAOAC bonds with hydroxyl side group formation [77]. Therefore, the reactive coupling agent successfully established strong chemical ‘‘bridges” between the biopolymer and sepiolite by SiAOAC bonds. As a result it generated a new hybrid nanostructure, i.e., a sepiolite-grafted P(3HB-co-4HB) (sepiolite-g-P(3HB-co-4HB)) nanocomposite.

3.3. Thermal properties

As previously discussed, both the crystallinity and thermal stability of P(3HB-co-4HB) have great influence on its performance. DSC was carried out to determine the influence of sepiolite nanoclay on the thermal properties of the P(3HB-co-4HB)

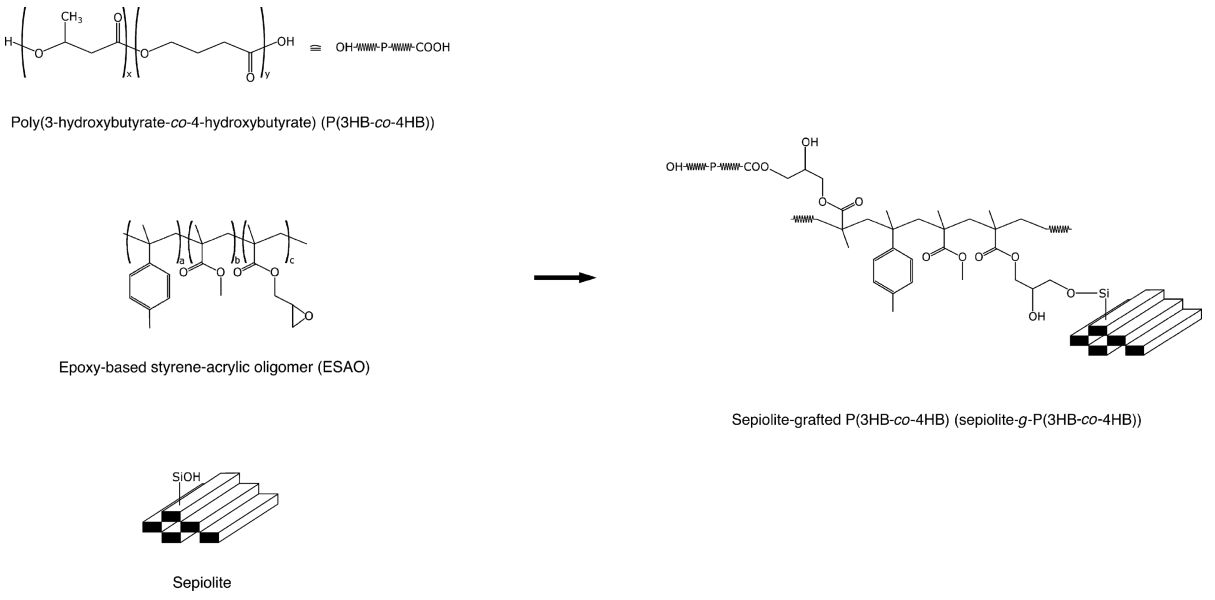

Fig. 3. Schematic representation of the melt grafting of sepiolite nanoclay onto poly(3-hydroxybutyrate-co-4-hydroxybutyrate) (P(3HB-co-4HB)) by epoxybased styrene-acrylic oligomer (ESAO).

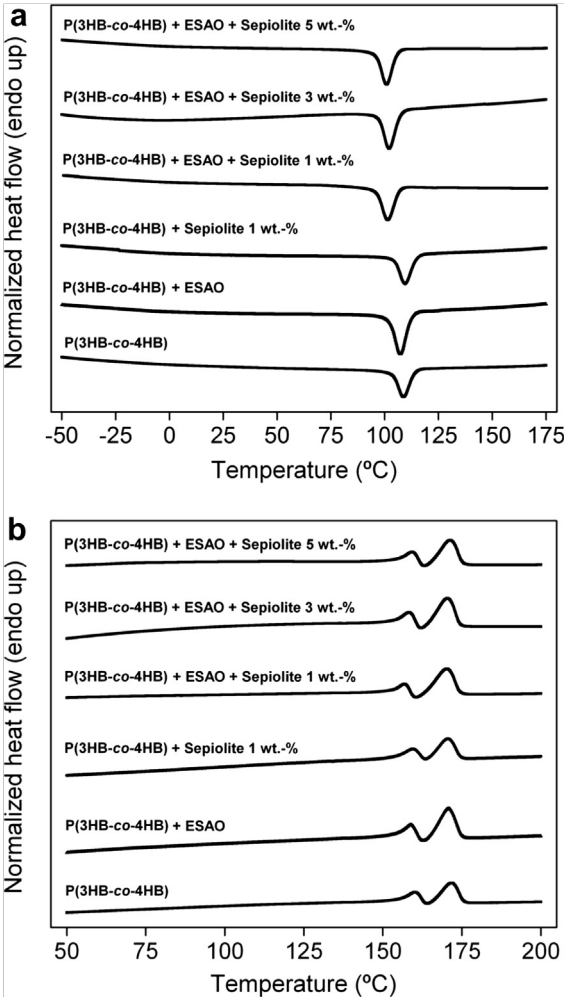

Fig. 4. Comparative plots of differential scanning calorimetry (DSC) thermograms for poly(3-hydroxybutyrate-co-4-hydroxybutyrate) (P(3HB-co-4HB)) nanocomposites containing sepiolite nanoclay and epoxy-based styrene-acrylic oligomer (ESAO) for: (a) First cooling run; (b) Second heating run.

nanocomposites. DSC thermograms for the first cooling and second heating scans are given in Fig. 4. Thermal values, obtained from the DSC thermograms, are collected in Table 2.

Table 2
Thermal properties obtained from the differential scanning calorimetry (DSC) and thermogravimetric analysis (TGA) curves in terms of normalized enthalpy of crystallization (ΔH_c), crystallization temperature from the melt (T_c), normalized enthalpy of melting (ΔH_m), melting temperature (T_m), amount of crystallinity (X_c), degradation temperature at 5% of mass loss ($T_{5\%}$), degradation temperature (T_{deg}), mass loss at T_{deg}, and residual mass for poly(3-hydroxybutyrate-*co*-4-hydroxybutyrate) (P(3HB-*co*-4HB)) nanocomposites containing epoxy-based styrene-acrylic oligomer (ESAO) and sepiolite nanoclay.

Samples	DSC							TGA			
	ΔH_c (J/g)	T_c (°C)	ΔH_{m1} (J/g)	T_{m1} (°C)	ΔH_{m2} (J/g)	T_{m2} (°C)	X_c (%)	$T_{5\%}$ (°C)	T_{deg} (°C)	Mass loss (%)	Residual mass (%)
P(3HB-*co*-4HB)	30.2 ± 0.8	109.1 ± 1.3	7.4 ± 0.3	160.1 ± 1.2	25.0 ± 0.2	171.3 ± 0.7	32.4 ± 1.7	289.7 ± 1.2	305.3 ± 1.4	36.1 ± 0.5	3.8 ± 0.3
P(3HB-*co*-4HB) + ESAO	33.4 ± 0.6	108.7 ± 0.9	9.4 ± 0.5	160.0 ± 1.3	27.1 ± 0.3	171.1 ± 1.3	36.2 ± 1.0	290.1 ± 1.0	305.1 ± 2.5	35.8 ± 0.4	3.9 ± 0.2
P(3HB-*co*-4HB) + Sepiolite 1 wt.-%	32.0 ± 0.5	109.8 ± 1.1	6.7 ± 0.5	159.3 ± 1.1	26.8 ± 0.7	170.2 ± 0.8	33.2 ± 1.6	290.3 ± 0.8	305.2 ± 1.9	33.4 ± 0.2	5.7 ± 0.1
P(3HB-*co*-4HB) + ESAO + Sepiolite 1 wt.-%	31.8 ± 0.7	102.5 ± 0.5	8.4 ± 0.4	157.9 ± 0.3	29.9 ± 0.6	169.7 ± 0.6	37.4 ± 0.2	291.4 ± 0.9	306.8 ± 1.7	38.5 ± 0.3	5.0 ± 0.2
P(3HB-*co*-4HB) + ESAO + Sepiolite 3 wt.-%	33.9 ± 0.6	101.9 ± 0.8	12.8 ± 0.7	157.6 ± 0.7	24.7 ± 0.1	169.7 ± 0.9	36.5 ± 0.6	292.3 ± 0.5	309.7 ± 0.9	41.6 ± 0.9	6.5 ± 0.1
P(3HB-*co*-4HB) + ESAO + Sepiolite 5 wt.-%	31.9 ± 0.4	101.2 ± 0.2	15.6 ± 0.6	157.6 ± 0.4	19.9 ± 0.1	169.6 ± 0.4	34.4 ± 0.9	292.4 ± 0.7	310.0 ± 1.1	44.2 ± 0.8	7.4 ± 0.1

Fig. 4a shows the cooling scans for P(3HB-co-4HB) and its nanocomposites. All samples showed crystallization from the melt during the cooling process, however this occurred at different temperatures. The unfilled biopolymer showed a T_c of about 109.1 C, which is in agreement with the previous study done by Dagnon et al. [78]. For the ungrafted P(3HB-co4HB) nanocomposite containing sepiolite at 1 wt.-%, T_c remained constant. However, T_c was found to decrease up to 101.2 C in the sepiolite-g-P(3HB-co-4HB) nanocomposites. These results indicated that sepiolite nanoclay, when melt grafted, certainly disrupted the ordering of P(3HB-co-4HB) by hindering chain diffusion and folding into the crystalline lattice. In the second heating scan, shown in Fig. 4b, all P(3HB-co-4HB) samples showed negligible cold crystallization. This is known to occur by the formation of imperfect crystals from unmelted ones acting as nuclei [79]. The heating thermogram of P(3HB-co-4HB) showed a bimodal endothermic peak: A first melting temperature at ca. 160.1 C followed by a more intense second melting temperature at ca. 171.3 C. Similar observations were previously found by Zhang et al. [80]. Multiple melting peaks in P(3HB-co-4HB) are certainly linked to crystal reorganization upon melting, by which imperfect crystals can order into spherulites with thicker lamellar thicknesses and then melt at higher temperatures. Lower melting peaks for P(3HB-co-4HB), which could be assigned to the crystalline phase of the 4HB-rich fractions [81,82], were not observed due to the relatively low 4HB mol.-% content. As shown in Table 2, melting temperatures of the P(3HB-co-4HB) nanocomposites slightly decreased with sepiolite. This can be attributed to a confinement effect of the nanoclay, which promoted less ordered structures.

Crystallinity values were calculated from DH_m evolved during the second heating scan. Table 2 shows that the resultant amount of crystallinity of P(3HB-co-4HB) increased from 32.4 to 36.2% with the addition of ESAO. This can be related to a M_W

improvement due to linear chain extension of P(3HB-co-4HB) and/or prevention of random chain scission reactions (e.g., hydrolysis) by which more mass of biopolymer crystallized [83]. Crystallinity was seen to slightly increase for a low content of sepiolite, i.e., 37.4% at 1 wt.-%, and then decreased for higher contents, i.e., 36.5 and 34.4% at 3 and 5 wt.-%, respectively. This suggests that crystal growth in the sepiolite-g-P(3HB-co-4HB) nanocomposites was controlled by two competing factors related to the nanoclay, i.e., the nucleation and confinement. The observed increase in crystallinity at the lowest sepiolite content indicates a dominant influence of the heterogeneous nucleation. At higher concentrations, however, certain agglomerations of sepiolite nanoparticles probably led to an excessive confinement that hindered molecular organization at the crystal growth front.

Relevant decomposition parameters, obtained from the TGA curves for P(3HB-co-4HB) and its nanocomposites, are also tabulated in Table 2. Thermal degradation of all P(3HB-co-4HB) materials occurred through a single and sharp degradation step that ranged from about 290 to 315 C. For the unfilled P(3HB-co-4HB) biopolymer, $T_{5\%}$ and T_{deg} were observed at ca. 289.7 and 305.3 C, respectively. The single introduction of ESAO or pristine sepiolite had a negligible effect on the decomposition profile of P(3HB-co-4HB). Conversely, as shown in the table, grafted sepiolite slightly delayed the degradation temperature of P(3HB-co-4HB). For instance, in the sepiolite-g-P(3HB-co-4HB) 3 wt.-% nanocomposite, $T_{5\%}$ and T_{deg} increased to 292.3 and 309.7 C, respectively. This effect can be mainly ascribed to a mass transport barrier exerted by the nanoclay to the volatiles produced during decomposition [6]. Due to the high porosity of sepiolite, certain sorption during degradation could be also responsible for delaying the sample weight loss [12]. For instance, thermal stability of PLA in nitrogen was improved around 16 C by addition of 5 wt.-% unmodified sepiolite [28]. In general, thermal degradation temperature of the sepioliteg-P(3HB-co-4HB) nanocomposites significantly exceeds the processing temperature and their thermal stability can meet the requirement of the industrial production by injection molding.

As also shown in Table 2, thermal degradation of unfilled P(3HB-co-4HB) was accompanied by the production of a residue of ca. 3.8% at 800 C. This can be related to microbial residues after polymerization as well as small amounts of additives added during polymer production. The residual mass increased in the P(3HB-co-4HB) nanocomposites with increasing the sepiolite content, which is known to produce a weight loss of ca. 20% at 850 C [32,40,49]. It is also worthy to mention that the addition of sepiolite nanoclay accelerated the weight loss rate of P(3HB-co-4HB), i.e., the percentage of mass loss increased with the degradation temperature. This confirmed that the nanoclay can function as a catalyst by which thermal degradation is accelerated [39]. A strong catalytic effect on the degradation of polyolefins by sepiolite has been also reported [27], underlining the drawbacks of the large presence of silanol groups on its surface.

3.4. Thermomechanical properties

Fig. 5 presents the temperature dependence expressed in terms of the storage modulus and tan d of neat P(3HB-co-4HB) and the various nanocomposites. The storage modulus represents the stiffness of a viscoelastic material and it is proportional to the energy stored during a loading cycle. As shown in Fig. 5a, DMTA curves of P(3HB-co-4HB) distinguished two processes. In the temperature range from 50 to 25 C, the storage modulus showed a significant decrease with increasing temperature. This is associated with the glass transition and it reflects the motions in connection with the biopolymer chains in the amorphous regions. From 25 C, the modulus presented a smoother decrease with temperature. This is originated from the chain mobility between the crystalline and amorphous regions, which depends on the lamellae thickness of the biopolymer. In this sense, Dagnon et al. [78] showed that P(3HB-co-4HB) exhibits two transitions at around 104 and 2 C, corresponding to beta (b) and alpha (a) relaxation processes, respectively. The b-relaxation (T_b) of the biopolymer is

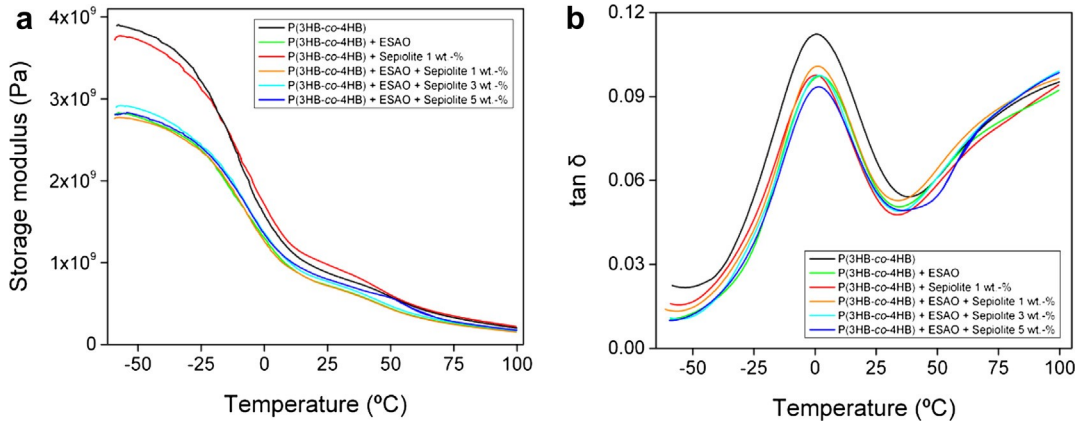

Fig. 5. Dynamic mechanical thermal analysis (DMTA) curves for poly(3-hydroxybutyrate-co-4-hydroxybutyrate) (P(3HB-co-4HB)) nanocomposites containing sepiolite nanoclay and epoxy-based styrene-acrylic oligomer (ESAO) for: (a) Storage modulus vs. temperature; (b) Damping factor (tan d) vs. temperature.

conventionally associated with local crankshaft motion of the $(CH_2)_n$ segment [84] whereas the a-relaxation constitutes the T_g of the biopolymer. It can be seen that the storage modulus decreased after the addition of ESAO at both glassy and rubbery states. This reduction was much more intense in the glassy state, i.e., at 50 C. The incorporation of sepiolite slightly increased the elastic properties of the P(3HB-co-4HB) matrix, which was more noticeable above 25 C. From 50 C, the modulus of the sepiolite-g-P(3HB-co-4HB) nanocomposites was similar than the neat biopolymer.

Tan d is defined as the ratio of loss modulus to storage modulus. It is a measure of the energy lost, expressed in terms of recoverable energy, which represents the mechanical damping or internal friction in a viscoelastic system. Tan d plots in Fig. 5b showed that the neat P(3HB-co-4HB) exhibits a well-resolved single relaxation peak with a maximum value at ca. 0.7 C, which defines the a-relaxation of the biopolymer. The incorporation of ESAO into P(3HB-co-4HB) slightly shifted the value to ca. 1.8 C. This effect can be associated with a slight reduction of chain mobility due to chain length extension. Sepiolite showed negligible variation at both peak shift and broadening of P(3HB-co-4HB) chain dynamics during glass transition. However, intensity values of tan d were reduced in the sepiolite-g-P(3HB-co-4HB) nanocomposites. Depression in the mechanical loss peak heights implies a reduction in the number of the mobile chains during the glass transition [85].

3.5. Mechanical properties

The tensile and flexural stress-strain curves of P(3HB-co-4HB) and its various nanocomposites are represented in Fig. 6. Table 3 includes the main mechanical values for each sample. It can be seen that the neat biopolymer behaves as an elastic material with a relatively low plastic deformation. The tensile modulus, strength, and elongation at break of P(3HB-co-4HB) were 689.3 MPa, 17.8 MPa, and 3.9%, respectively. In relation to the flexural properties, the flexural modulus, strength, and elongation at break were 1226 MPa, 27.4 MPa, and 3.8%, respectively. Similar mechanical values for injection-molded parts were obtained by Zhang et al. [80], who particularly reported a tensile strength at yield of about 17.5 MPa and an elongation at break below 5%. Notable enhancements in stiffness and yield stress were observed with the addition of ESAO, which can be related to the M_W improvement in the biopolymer structure. Elastic moduli of the P(3HB-co-4HB) nanocomposites also increased with the sepiolite content in the investigated concentration range, indicating that the nanoclay effectively enhanced the material stiffness. In particular, the sepiolite-g-P(3HB-co-4HB) 5 wt.-% nanocomposite increased the tensile modulus and strength up to 1012.1 and 21.9 MPa, respectively. The flexural modulus and strength also increased to 1635.6 and 29.8 MPa, respectively. In the case of the tensile and flexural moduli, this represents a percentage increase of about 47 and 35%, respectively.

The high reinforcement generated by sepiolite suggests that a good dispersion level of the nanoclay in the biopolymer matrix was reached. Indeed, without an effective interaction between the P(3HB-co-4HB) matrix and sepiolite, the nanoclay would act as a merely stress concentrator, i.e., the so-called ‘‘notch effect”. In agreement with previous studies, the high content of silanol groups exposed on the external surface of sepiolite can favor its compatibilization with polycondensation polymers such as polyesters and polyamides. For instance, the tensile modulus and yield strength of PA 66 was increased from 2.06 to 2.73 GPa and from 53.7 to 60.9 MPa, respectively, with 5 wt.-% of sepiolite in the study performed by Fernandez-Barranco et al. [36]. However, in the same study, the elongation-at-break value drastically decreased from 182 to 42%. In the research work carried out by Sabzi et al. [46], the incorporation of unmodified sepiolite into PLA at 10 wt.-% led to a 25% increase in the tensile modulus. Notable mechanical reinforcements were also reported for nanocomposites based on starch [12], PA 6 [33,34], and gelatin [53], which proves that sepiolite can be effectively dispersed in polar

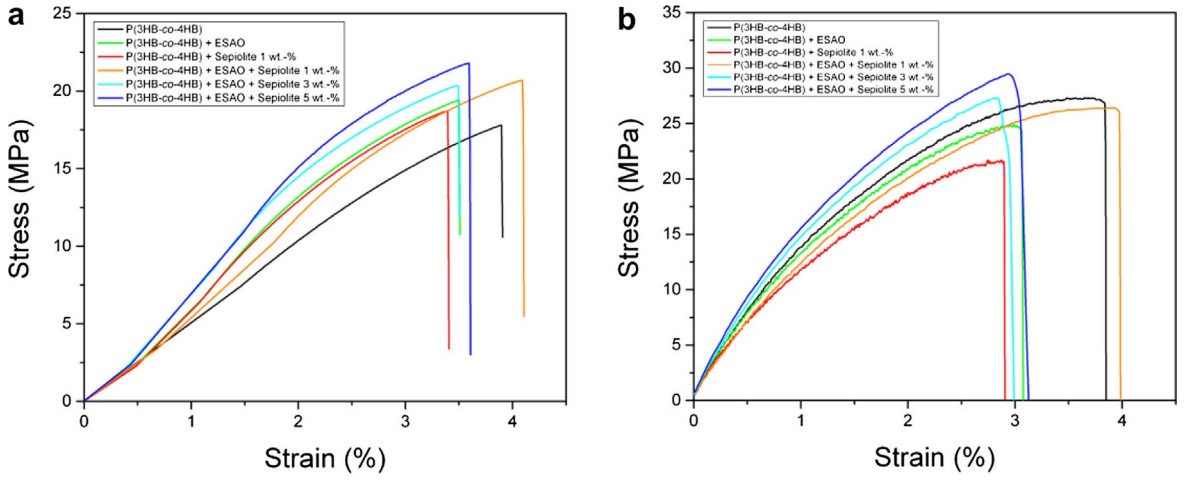

Fig. 6. Typical stress-strain curves of poly(3-hydroxybutyrate-co-4-hydroxybutyrate) (P(3HB-co-4HB)) nanocomposites containing sepiolite nanoclay and epoxy-based styrene-acrylic oligomer (ESAO) for: (a) Tensile tests; (b) Flexural tests.

Table 3

Mechanical properties in terms of tensile modulus ($E_{tensile}$), tensile strength at yield ($r_{tensile}$), tensile elongation at break ($e_{tensile}$), flexural modulus ($E_{flexural}$), flexural strength at yield ($r_{flexural}$), flexural elongation at break ($e_{flexural}$), Shore D hardness, and Charpy impact strength for poly(3-hydroxybutyrate-co-4hydroxybutyrate) (P(3HB-co-4HB)) nanocomposites containing epoxy-based styrene-acrylic oligomer (ESAO) and sepiolite nanoclay.

Samples	Tensile test			Flexural test			Shore D hardness	Charpy impact strength (kJ/m^2)
	$E_{tensile}$ (MPa)	$r_{tensile}$ (MPa)	$e_{tensile}$ (%)	$E_{flexural}$ (MPa)	$r_{flexural}$ (MPa)	$e_{flexural}$ (%)		
P(3HB-co-4HB)	689.3 ± 58.3	17.8 ± 0.9	3.9 ± 0.3	1226.0 ± 173.3	27.4 ± 2.9	3.8 ± 0.2	66.8 ± 1.3	3.0 ± 0.2
P(3HB-co-4HB) + ESAO	893.2 ± 60.2	19.4 ± 0.9	3.5 ± 0.3	1353.3 ± 154.1	24.9 ± 5.5	3.1 ± 0.4	67.0 ± 1.2	2.1 ± 0.5
P(3HB-co-4HB) + Sepiolite 1 wt.-%	897.0 ± 62.0	18.7 ± 0.9	3.3 ± 0.2	1207.8 ± 209.7	21.7 ± 3.7	2.9 ± 0.3	64.2 ± 2.0	2.1 ± 0.4
P(3HB-co-4HB) + ESAO + Sepiolite 1 wt.-%	938.1 ± 81.3	20.7 ± 0.8	4.1 ± 0.5	1381.9 ± 157.0	26.9 ± 3.6	4.0 ± 0.3	67.0 ± 0.7	2.4 ± 0.6
P(3HB-co-4HB) + ESAO + Sepiolite 3 wt.-%	977.6 ± 73.8	20.4 ± 1.1	3.5 ± 0.5	1489.0 ± 189.1	27.4 ± 4.3	3.0 ± 0.2	67.6 ± 0.5	2.2 ± 0.3
P(3HB-co-4HB) + ESAO + Sepiolite 5 wt.-%	1012.1 ± 51.9	21.9 ± 0.9	3.6 ± 0.2	1635.6 ± 165.5	29.8 ± 4.9	3.1 ± 0.5	69.4 ± 0.5	2.3 ± 0.6

polymer matrices by melt mixing. Nevertheless, it is also worthy to mention that, in most of the previous polymer nanocomposites, ductility decreased with increasing the sepiolite content. Indeed, in the present study the incorporation of 1 wt.-% of pristine sepiolite also reduced the elongation at break of P(3HB-co-4HB) from 3.9 to 3.3%. Interestingly, this strain reduction was not observed for the equivalent sepiolite-g-P(3HB-co-4HB) nanocomposite. The melt-grafted P(3HB-co-4HB) nanocomposites still preserved around 90% of the initial strain-at-break value, even at the highest sepiolite content, i.e., 5 wt.-%. This evidences that mechanical stress can be effectively transferred from sepiolite to the P(3HB-co-4HB) matrix due to melt grafting.

Table 3 also includes the mechanical values obtained from the Shore D hardness and Charpy impact tests. Hardness followed the same trend previously observed in the moduli, i.e., the addition of both ESAO and sepiolite exerted a positive effect on the properties of P(3HB-co-4HB). It was noticeable the low value observed for the ungrafted nanocomposite. This suggests that pristine sepiolite presents a poor interfacial adhesion with the biopolymer matrix. As opposite, the incorporation of sepiolite nanoclay reduced the impact strength of P(3HB-co-4HB). This is an expected consequence of the rigidity increase and loss of toughness in the P(3HB-co-4HB) nanocomposites. Sepiolite embrittled the P(3HB-co-4HB) matrix by immobilizing the biopolymer chains and constraining plastic deformation. Nevertheless, similar to the other mechanical properties, this impairment was attenuated for the P(3HB-co-4HB) nanocomposites produced by reactive extrusion. This indicates that the sepiolite-g-P(3HB-co-4HB) nanocomposites were able to absorb higher amounts of energy before fracture.

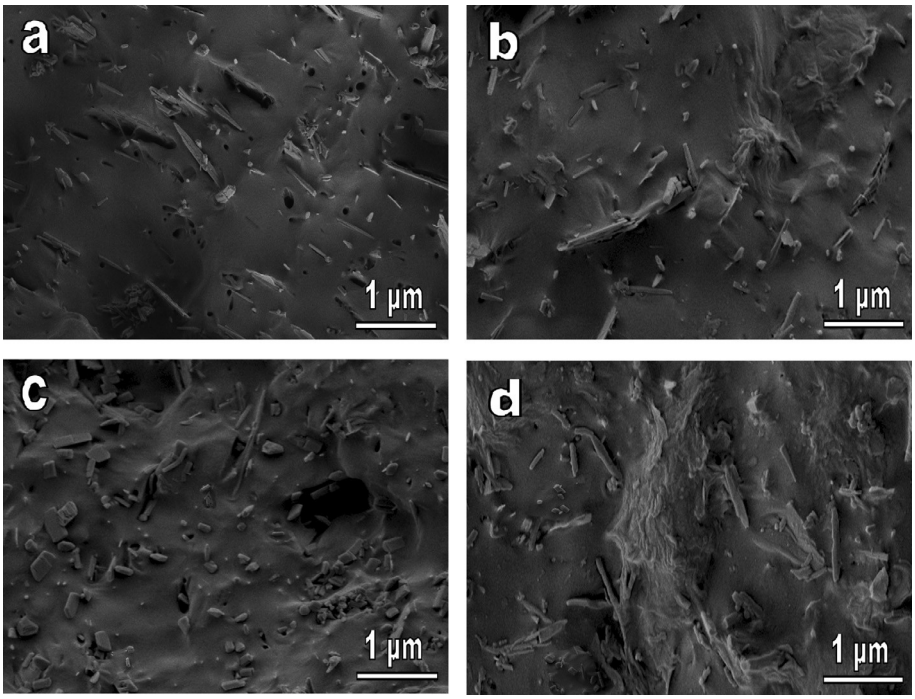

Fig. 7. Scanning electron microscope (SEM) images of the fractured surfaces of poly(3-hydroxybutyrate-co-4-hydroxybutyrate) (P(3HB-co-4HB)) nanocomposites based on: (a) Ungrafted sepiolite at 1 wt.-%; (b) Melt-grafted sepiolite at 1 wt.-%; (c) Melt-grafted sepiolite at 3 wt.-%; (d) Melt-grafted sepiolite at 5 wt.-%. Scale markers of 1 lm in all cases.

3.6. Morphology of nanocomposites

The fractured surfaces of the P(3HB-co-4HB) nanocomposites, after the Charpy impact tests, were analyzed by SEM. Micrographs included in Fig. 7 revealed the presence of sepiolite as needle-shaped structures embedded in the biopolymer matrix. All P(3HB-co-4HB) nanocomposites showed a high degree of dispersion and a relatively low

number of sepiolite aggregates, even at high contents of nanoclay. As above stated, this finding can be related to the good chemical affinity between the polar P(3HB-co-4HB) chains with the silanol groups of sepiolite. In Fig. 7a, which corresponds to the ungrafted P(3HB-co-4HB) nanocomposite, it is possible to identify spherical voids and fiber-like gaps that correspond to sepiolite nanoparticles that were removed from the biopolymer matrix after fracture. Interfacial debonding supports the previous mechanical results in which the P(3HB-co-4HB) nanocomposite produced without ESAO lacked of sufficient adhesion with the nanoclay. As a result the ungrafted samples were more prone to produce mechanical failures at low strains.

The effect of melt grafting can be observed in Fig. 7b for the sepiolite-g-P(3HB-co-4HB) 1 wt.-% nanocomposite. This sample showed no fracture lines located at the sepiolite-biopolymer interface and the number of voids after fracture was significantly reduced too. The melt-grafted P(3HB-co-4HB) nanocomposites containing higher amounts of sepiolite, i.e., 3 wt.-% (Fig. 7c) and 5 wt.-% (Fig. 7d), exhibited rougher and more irregular fracture surfaces. As it can be seen in these images, increasing the sepiolite content also produced some filler attrition, i.e., length reduction of sepiolite nanoparticles. This can be due to a higher number of nanofillers collision and increased shear stresses during melt compounding [86]. Additionally, sepiolite nanoparticles could also break during the mechanical test due to their strong interaction with the P(3HB-co4HB) matrix. In any case, an optimal distribution of sepiolite was achieved since single nanoparticles were effectively dispersed and no sepiolite bundles were observed even at the highest concentration.

4. Conclusions

Sepiolite-g-P(3HB-co-4HB) nanocomposites were successfully obtained by reactive extrusion using a multi-functional epoxy-based oligomer in a twin-screw extruder. Silanol groups on the external surface of the nanoclay effectively grafted onto the biopolymer via alkoxy silanes bonds. Sepiolite interaction with the biopolymer was detected in the FTIR spectra of the melt-grafted P(3HB-co-4HB) nanocomposites by the formation of SiAOAC bands in the region of 1100–1000 cm^1 and at 815 cm^1. Melt-grafted sepiolite improved the thermal stability and mechanical properties of P(3HB-co-4HB). In particular, T_{deg} was retarded about 5 C while the tensile and flexural moduli increased up to 47 and 35%, respectively, for the sepiolite-g-P(3HB-co-4HB) 5 wt.-% nanocomposite. Melt-grafted P(3HB-co-4HB) nanocomposites also retained around 90% of the elongation-at-break and impact-strength values. SEM analysis revealed that sepiolite was efficiently embedded in the P(3HB-co-4HB) matrix. Melt grafting was supported in the fractured surfaces by the absence of voids and high interfacial interaction between sepiolite and the biopolymer. Future studies should be focused on assessing the potential benefits of multi-functional epoxy-based additives to increase the processability of biodegradable polymer nanocomposites and their influence on the biodegradation behavior.

Melt compounding with highly reactive coupling agents can be regarded as a novel tool to develop high-performing polymer nanocomposites. In particular, melt grafting of nanoclays can potentially enhance the thermal and mechanical performance of biopolymers. This may promote and revolutionize their accessibility to industrial sectors such as packaging, where both good performance and environmental concerns are requirements.

Acknowledgements

The Spanish Ministry of Economy and Competitiveness is acknowledged for funding support through the research project MAT2014-59242-C2-1-R and the Torres Quevedo program of Dr. Torres-Giner (PTQ-11-04733). Quiles-Carrillo also thanks ‘‘Generalitat Valenciana” for his FPI grant (ACIF/2016/182). The authors thank Pr. Chris Sammon from Sheffield Hallam University for his support during FTIR characterization.

References

[1] S. Nakamura, Y. Doi, M. Scandola, Microbial synthesis and characterization of poly(3-hydroxybutyrate-co-4-hydroxybutyrate), Macromolecules 25 (17) (1992) 4237–4241.

[2] M. Kunioka, A. Tamaki, Y. Doi, Crystalline and thermal properties of bacterial copolyesters: poly(3-hydroxybutyrate-co-3-hydroxyvalerate) and poly(3hydroxybutyrate-co-4-hydroxybutyrate), Macromolecules 22 (2) (1989) 694–697.
[3] Y. Saito, S. Nakamura, M. Hiramitsu, Y. Doi, Microbial synthesis and properties of poly(3-hydroxybutyrate-co-4-hydroxybutyrate), Polym. Int. 39 (3) (1996) 169–174.
[4] S. Philip, T. Keshavarz, I. Roy, Polyhydroxyalkanoates: biodegradable polymers with a range of applications, J. Chem. Technol. Biotechnol. 82 (3) (2007) 233–247.
[5] L.J. Han, C.Y. Han, W.L. Cao, X.M. Wang, J.J. Bian, L.S. Dong, Preparation and characterization of biodegradable poly(3-hydroxybutyrate-co-4hydroxybutyrate)/silica nanocomposites, Polym. Eng. Sci. 52 (2) (2012) 250–258.
[6] X. Wang, H. Zhang, M. Liu, D. Jia, Thermal stability of poly(3-hydroxybutyrate-co-4-hydroxybutyrate)/modified montmorillonite bio-nanocomposites, Polym. Compos. (2015), http://dx.doi.org/10.1002/pc.23626.
[7] J.L. Feijoo-Gomez, S. Torres-Giner, C. Vázquez-Torner, INNOVEX a new technology for masterbatch additives for the XPS industry, in: 10th International Conference on Foam Materials and Technology, FOAMS 2012, Society of Plastics Engineers, 2012, pp. 101–104.
[8] S. Torres-Giner, A. Martinez-Abad, J.M. Lagaron, Zein-based ultrathin fibers containing ceramic nanofillers obtained by electrospinning. II. Mechanical properties, gas barrier, and sustained release capacity of biocide thymol in multilayer polylactide films, J. Appl. Polym. Sci. 131 (18) (2014) 9270–9276.
[9] H. Angellier-Coussy, S. Torres-Giner, M.H. Morel, N. Gontard, E. Gastaldi, Functional properties of thermoformed wheat gluten/montmorillonite materials with respect to formulation and processing conditions, J. Appl. Polym. Sci. 107 (1) (2008) 487–496.
[10] E. Bilotti, H.R. Fischer, T. Peijs, Polymer nanocomposites based on needle-like sepiolite clays: effect of functionalized polymers an the dispersion of nanofiller, crystallinity, and mechanical properties, J. Appl. Polym. Sci. 107 (2) (2008) 1116–1123.
[11] E. Duquesne, S. Moins, M. Alexandre, P. Dubois, How can nanohybrids enhance polyester/sepiolite nanocomposite properties?, Macromol Chem. Phys. 208 (23) (2007) 2542–2550.
[12] F. Chivrac, E. Pollet, M. Schmutz, L. Averous, Starch nano-biocomposites based on needle-like sepiolite clays, Carbohydr. Polym. 80 (1) (2010) 145–153.
[13] M. Darder, M. Lopez-Blanco, P. Aranda, A.J. Aznar, J. Bravo, E. Ruiz-Hitzky, Microfibrous chitosan-sepiolite nanocomposites, Chem. Mater. 18 (6) (2006) 1602–1610.
[14] R. Benlikaya, M. Alkan, I. Kaya, Preparation and characterization of sepiolite-poly(ethyl methacrylate) and poly(2-hydroxyethyl methacrylate) nanocomposites, Polym. Compos. 30 (11) (2009) 1585–1594.
[15] P. Aranda, R. Kun, M.A. Martin-Luengo, S. Letaief, I. Dekany, E. Ruiz-Hitzky, Titania-sepiolite nanocomposites prepared by a surfactant templating colloidal route, Chem. Mater. 20 (1) (2008) 84–91.
[16] A.K. Helmy, S.G. de Bussetti, The surface properties of sepiolite, Appl. Surf. Sci. 255 (5) (2008) 2920–2924.
[17] A. Mejia, N. Garcia, J. Guzman, P. Tiemblo, Confinement and nucleation effects in poly(ethylene oxide) melt-compounded with neat and coated sepiolite nanofibers: modulation of the structure and semicrystalline morphology, Eur. Polym. J. 49 (1) (2013) 118–129.
[18] G. Tartaglione, D. Tabuani, G. Camino, M. Moisio, PP and PBT composites filled with sepiolite: morphology and thermal behaviour, Compos. Sci. Technol. 68 (2) (2008) 451–460.
[19] E. Galan, Properties and applications of palygorskite-sepiolite clays, Clay Miner. 31 (4) (1996) 443–453.
[20] M.C. Hermosin, J. Cornejo, Methylation of sepiolite and palygorskite with diazomethane, Clays Clay Miner. 34 (5) (1986) 591–596.
[21] N. Volle, F. Giulieri, A. Burr, S. Pagnotta, A.M. Chaze, Controlled interactions between silanol groups at the surface of sepiolite and an acrylate matrix: consequences on the thermal and mechanical properties, Mater. Chem. Phys. 134 (1) (2012) 417–424.
[22] M.D. Samper-Madrigal, O. Fenollar, F. Dominici, R. Balart, J.M. Kenny, The effect of sepiolite on the compatibilization of polyethylene-thermoplastic starch blends for environmentally friendly films, J. Mater. Sci. 50 (2) (2015) 863–872.
[23] J. Ma, E. Bilotti, T. Peijs, J.A. Darr, Preparation of polypropylene/sepiolite nanocomposites using supercritical CO2 assisted mixing, Eur. Polym. J. 43 (12) (2007) 4931–4939.
[24] E. Bilotti, H. Deng, R. Zhang, D. Lu, W. Bras, H.R. Fischer, T. Peijs, Synergistic reinforcement of highly oriented poly(propylene) tapes by sepiolite nanoclay, Macromol. Mater. Eng. 295 (1) (2010) 37–47.
[25] A.F. Vargas, V.H. Orozco, F. Rault, S. Giraud, E. Devaux, B.L. Lopez, Influence of fiber-like nanofillers on the rheological, mechanical, thermal and fire properties of polypropylene an application to multifilament yarn, Compos. Part A-Appl. Sci. Manuf. 41 (12) (2010) 1797–1806.
[26] S. Pappalardo, P. Russo, D. Acierno, S. Rabe, B. Schartel, The synergistic effect of organically modified sepiolite in intumescent flame retardant polypropylene, Eur. Polym. J. 76 (2016) 196–207.
[27] A. Marcilla, A. Gomez, S. Menargues, R. Ruiz, Pyrolysis of polymers in the presence of a commercial clay, Polym. Degrad. Stab. 88 (3) (2005) 456–460. [28] K. Fukushima, D. Tabuani, G. Camino, Nanocomposites of PLA and PCL based on montmorillonite and sepiolite, Mater. Sci. Eng. C-Biomimetic Supramol. Syst. 29 (4) (2009) 1433–1441.
[29] K. Fukushima, D. Tabuani, C. Abbate, M. Arena, L. Ferreri, Effect of sepiolite on the biodegradation of poly(lactic acid) and polycaprolactone, Polym. Degrad. Stab. 95 (10) (2010) 2049–2056.
[30] N. Garcia, M. Hoyos, J. Guzman, P. Tiemblo, Comparing the effect of nanofillers as thermal stabilizers in low density polyethylene, Polym. Degrad. Stab. 94 (1) (2009) 39–48.
[31] M. Shafiq, T. Yasin, S. Saeed, Synthesis and characterization of linear low-density polyethylene/sepiolite nanocomposites, J. Appl. Polym. Sci. 123 (3) (2012) 1718–1723.
[32] D. Garcia-Lopez, J.F. Fernandez, J.C. Merino, J. Santaren, J.M. Pastor, Effect of organic modification of sepiolite for PA 6 polymer/organoclay nanocomposites, Compos. Sci. Technol. 70 (10) (2010) 1429–1436.
[33] E. Bilotti, R. Zhang, H. Deng, F. Quero, H.R. Fischer, T. Peijs, Sepiolite needle-like clay for PA6 nanocomposites: an alternative to layered silicates?, Compos Sci. Technol. 69 (15–16) (2009) 2587–2595.

[34] S. Xie, S. Zhang, F. Wang, M. Yang, R. Séguéla, J.-M. Lefebvre, Preparation, structure and thermomechanical properties of nylon-6 nanocomposites with lamella-type and fiber-type sepiolite, Compos. Sci. Technol. 67 (11–12) (2007) 2334–2341.
[35] D. Garcia-Lopez, J.F. Fernandez, J.C. Merino, J.M. Pastor, Influence of organic modifier characteristic on the mechanical properties of polyamide 6/ organosepiolite nanocomposites, Compos. Part B-Eng. 45 (1) (2013) 459–465.
[36] C. Fernandez-Barranco, A. Yebra-Rodriguez, M.D. La Rubia-Garcia, F.J. Navas-Martos, P. Alvarez-Lloret, Mechanical and crystallographic properties of injection-molded polyamide 66/sepiolite nanocomposites with different clay loading, Polym. Compos. 36 (12) (2015) 2326–2333.
[37] C. Fernandez-Barranco, A.E. Koziol, K. Skrzypiec, M. Rawski, M. Drewniak, A. Yebra-Rodriguez, Study of spatial distribution of sepiolite in sepiolite/ polyamide6,6 nanocomposites, Appl. Clay. Sci. 127 (2016) 129–133.
[38] Y. Yu, S.L. Qi, J.Y. Zhan, Z.P. Wu, X.P. Yang, D.Z. Wu, Polyimide/sepiolite nanocomposite films: preparation, morphology and properties, Mater. Res. Bull. 46 (10) (2011) 1593–1599.
[39] H. Chen, M. Zheng, H. Sun, Q. Jia, Characterization and properties of sepiolite/polyurethane nanocomposites, Mater. Sci. Eng., A 445–446 (2007) 725– 730.
[40] H. Chen, H. Lu, Y. Zhou, M. Zheng, C. Ke, D. Zeng, Study on thermal properties of polyurethane nanocomposites based on organo-sepiolite, Polym. Degrad. Stab. 97 (3) (2012) 242–247.
[41] H. Chen, D. Zeng, X. Xiao, M. Zheng, C. Ke, Y. Li, Influence of organic modification on the structure and properties of polyurethane/sepiolite nanocomposites, Mater. Sci. Eng., A 528 (3) (2011) 1656–1661.
[42] A. Nohales, L. Solar, I. Porcar, C.I. Vallo, C.M. Gomez, Morphology, flexural, and thermal properties of sepiolite modified epoxy resins with different curing agents, Eur. Polym. J. 42 (11) (2006) 3093–3101.
[43] A. Nohales, R. Munoz-Espi, P. Felix, C.M. Gomez, Sepiolite-reinforced epoxy nanocomposites: thermal, mechanical, and morphological behavior, J. Appl. Polym. Sci. 119 (1) (2011) 539–547.
[44] E. Franchini, J. Galy, J.F. Gerard, Sepiolite-based epoxy nanocomposites: relation between processing, rheology, and morphology, J. Colloid Interface Sci. 329 (1) (2009) 38–47.
[45] T.D. Hapuarachchi, T. Peijs, Multiwalled carbon nanotubes and sepiolite nanoclays as flame retardants for polylactide and its natural fibre reinforced composites, Compos. Part A-Appl. Sci. Manuf. 41 (8) (2010) 954–963.
[46] M. Sabzi, L. Jiang, M. Atai, I. Ghasemi, PLA/sepiolite and PLA/calcium carbonate nanocomposites: a comparison study, J. Appl. Polym. Sci. 129 (4) (2013) 1734–1744.
[47] E. Nieddu, L. Mazzucco, P. Gentile, T. Benko, V. Balbo, R. Mandrile, G. Ciardelli, Preparation and biodegradation of clay composites of PLA, React. Funct. Polym. 69 (6) (2009) 371–379.
[48] K. Fukushima, D. Tabuani, G. Camino, Poly(lactic acid)/clay nanocomposites: effect of nature and content of clay on morphology, thermal and thermomechanical properties, Mater. Sci. Eng. C-Mater. Biol. Appl. 32 (7) (2012) 1790–1795.
[49] K. Fukushima, A. Fina, F. Geobaldo, A. Venturello, G. Camino, Properties of poly(lactic acid) nanocomposites based on montmorillonite, sepiolite and zirconium phosphonate, Express Polym. Lett. 6 (11) (2012) 914–926.
[50] K. Fukushima, A. Rasyida, M.C. Yang, Characterization, degradation and biocompatibility of PBAT based nanocomposites, Appl. Clay. Sci. 80–81 (2013) 291–298.
[51] L. Bokobza, A. Burr, G. Garnaud, M.Y. Perrin, S. Pagnotta, Fibre reinforcement of elastomers: nanocomposites based on sepiolite and poly(hydroxyethyl acrylate), Polym. Int. 53 (8) (2004) 1060–1065.
[52] M. Frydrych, C.Y. Wan, R. Stengler, K.U. O'Kelly, B.Q. Chen, Structure and mechanical properties of gelatin/sepiolite nanocomposite foams, J. Mater. Chem. 21 (25) (2011) 9103–9111.
[53] F. Miguel Fernandes, A. Isabel Ruiz, M. Darder, P. Aranda, E. Ruiz-Hitzky, Gelatin-clay bio-nanocomposites: structural and functional properties as advanced materials, J. Nanosci. Nanotechnol. 9 (1) (2009) 221–229.
[54] M.F. Can, L. Avdan, A.C. Bedeloglu, Properties of biodegradable PVA/sepiolite-based nanocomposite fiber mats, Polym. Compos. 36 (12) (2015) 2334– 2342.
[55] F. Santiago, A.E. Mucientes, M. Osorio, F.J. Poblete, Synthesis and swelling behaviour of poly(sodiurn acrylate)/sepiolite superabsorbent composites and nanocomposites, Polym. Int. 55 (8) (2006) 843–848.
[56] S. Mir, T. Yasin, P.J. Halley, H.M. Siddiqi, O. Ozdemir, A. Nguyen, Thermal and rheological effects of sepiolite in linear low-density polyethylene/starch blend, J. Appl. Polym. Sci. 127 (2) (2013) 1330–1337.
[57] K. Nunez, C. Rosales, R. Perera, N. Villarreal, J.M. Pastor, Poly(lactic acid)/low-density polyethylene blends and its nanocomposites based on sepiolite, Polym. Eng. Sci. 52 (5) (2012) 988–1004.
[58] K. Nunez, C. Rosales, R. Perera, N. Villarreal, J.M. Pastor, Nanocomposites of PLA/PP blends based on sepiolite, Polym. Bull. 67 (9) (2011) 1991–2016.
[59] J.B. Olivato, J. Marini, E. Pollet, F. Yamashita, M.V.E. Grossmann, L. Averous, Elaboration, morphology and properties of starch/polyester nanobiocomposites based on sepiolite clay, Carbohydr. Polym. 118 (2015) 250–256.
[60] R.L. Frost, E. Mendelovici, Modification of fibrous silicates surfaces with organic derivatives: an infrared spectroscopic study, J. Colloid Interface Sci. 294 (1) (2006) 47–52.
[61] S. Duangphet, D. Szegda, J. Song, K. Tarverdi, The effect of chain extender on poly(3-hydroxybutyrate-co-3-hydroxyvalerate): thermal degradation, crystallization, and rheological behaviours, J. Polym. Environ. 22 (1) (2014) 1–8.
[62] L.C. Arruda, M. Magaton, R.E.S. Bretas, M.M. Ueki, Influence of chain extender on mechanical, thermal and morphological properties of blown films of PLA/PBAT blends, Polym. Testing 43 (2015) 27–37.
[63] M. Villalobos, A. Awojulu, T. Greeley, G. Turco, G. Deeter, Oligomeric chain extenders for economic reprocessing and recycling of condensation plastics, Energy 31 (15) (2006) 3227–3234.

[64] X. Wen, X. Lu, Q. Peng, F. Zhu, N. Zheng, Crystallization behaviors and morphology of biodegradable poly(3-hydroxybutyrate-co-4-hydroxybutyrate), J. Therm. Anal. Calorim. 109 (2) (2012) 959–966.
[65] S. Torres-Giner, Electrospun nanofibers for food packaging applications, Multifunctional and Nanoreinforced Polymers for Food Packaging, 5, Woodhead Publishing Limited, 2011, pp. 108–125.
[66] T.C. Chang, P.T. Liu, Y.S. Mor, S.M. Sze, Y.L. Yang, M.S. Feng, F.M. Pan, B.T. Dai, C.Y. Chang, The novel improvement of low dielectric constant methylsilsesquioxane by N2O plasma treatment, J. Electrochem. Soc. 146 (10) (1999) 3802–3806.
[67] Y. Wang, C. Fu, Y. Luo, C. Ruan, Y. Zhang, Y. Fu, Melt synthesis and characterization of poly(L-lactic acid) chain linked by multifunctional epoxy compound, J. Wuhan Univ. Technol.-Mater. Sci. Ed. 25 (5) (2010) 774–779.
[68] D. Wei, H. Wang, H. Xiao, A. Zheng, Y. Yang, Morphology and mechanical properties of poly(butylene adipate-co-terephthalate)/potato starch blends in the presence of synthesized reactive compatibilizer or modified poly(butylene adipate-co-terephthalate), Carbohydr. Polym. 123 (2015) 275–282.
[69] M.A. Abdelwahab, S. Taylor, M. Misra, A.K. Mohanty, Thermo-mechanical characterization of bioblends from polylactide and poly(butylene adipate-coterephthalate) and lignin, Macromol. Mater. Eng. 300 (3) (2015) 299–311.
[70] L.H. Guo, H. Sato, T. Hashimoto, Y. Ozaki, FTIR study on hydrogen-bonding interactions in biodegradable polymer blends of poly(3-hydroxybutyrate) and poly(4-vinylphenol), Macromolecules 43 (8) (2010) 3897–3902.
[71] H. Sato, R. Murakami, A. Padermshoke, F. Hirose, K. Senda, I. Noda, Y. Ozaki, Infrared spectroscopy studies of CHO hydrogen bondings and thermal behavior of biodegradable poly(hydroxyalkanoate), Macromolecules 37 (19) (2004) 7203–7213.
[72] H. Huang, Y. Hu, J.M. Zhang, H. Sato, H.T. Zhang, I. Noda, Y. Ozaki, Miscibility and hydrogen-bonding interactions in biodegradable polymer blends of poly(3-hydroxybutyrate) and a partially hydrolyzed poly(vinyl alcohol), J. Phys. Chem. B 109 (41) (2005) 19175–19183.
[73] Q.R. Sun, T. Mekonnen, M. Misra, A.K. Mohanty, Novel biodegradable cast film from carbon dioxide based copolymer and poly(lactic acid), J. Polym. Environ. 24 (1) (2016) 23–36.
[74] S.Y. Jing, H.J. Lee, C.K. Choi, Chemical bond structure on Si-O-C composite films with a low dielectric constant deposited by using inductively coupled plasma chemical vapor deposition, J. Korean Phys. Soc. 41 (5) (2002) 769–773.
[75] C.S. Yang, K.S. Oh, J.Y. Ryu, D.C. Kim, J. Shou-Yong, C.K. Choi, H.-J. Lee, S.H. Um, H.Y. Chang, A study on the formation and characteristics of the SiOCH composite thin films with low dielectric constant for advanced semiconductor devices, Thin Solid Films 390 (1–2) (2001) 113–118.
[76] R. Al-Itry, K. Lamnawar, A. Maazouz, Improvement of thermal stability, rheological and mechanical properties of PLA, PBAT and their blends by reactive extrusion with functionalized epoxy, Polym. Degrad. Stab. 97 (10) (2012) 1898–1914.
[77] Y.-M. Corre, J. Duchet, J. Reignier, A. Maazouz, Melt strengthening of poly (lactic acid) through reactive extrusion with epoxy-functionalized chains, Rheol. Acta 50 (7) (2011) 613–629.
[78] K.L. Dagnon, C. Thellen, J.A. Ratto, N.A. D'Souza, Physical and thermal analysis of the degradation of poly(3-hydroxybutyrate-co-4-hydroxybutyrate) coated paper in a constructed soil medium, J. Polym. Environ. 18 (4) (2010) 510–522.
[79] Y.X. An, L.S. Dong, L.X. Li, Z.S. Mo, Z.L. Feng, Isothermal crystallization kinetics and melting behavior of poly(beta-hydroxybutyrate)/poly(vinyl acetate) blends, Eur. Polym. J. 35 (3) (1999) 365–369.
[80] K. Zhang, M. Misra, A.K. Mohanty, Toughened sustainable green composites from poly(3-hydroxybutyrate-co-3-hydroxyvalerate) based ternary blends and miscanthus biofiber, ACS Sustainable Chem. Eng. 2 (10) (2014) 2345–2354.
[81] W. Hsieh, H. Mitomo, K. Kasuya, T. Komoto, Enzymatic degradation and aminolysis of microbial poly(3-hydroxybutyrate-co-4-hydroxybutyrate) single crystals, J. Polym. Environ. 14 (1) (2006) 79–87.
[82] C.B. Cong, S.Y. Zhang, R.W. Xu, W.C. Lu, D.S. Yu, The influence of 4HB content on the properties of poly(3-hydroxylbutyrate-co-4-hydroxylbutyrate) based on melt molded sheets, J. Appl. Polym. Sci. 109 (3) (2008) 1962–1967.
[83] M. Erceg, T. Kovacic, I. Klaric, Thermal degradation of poly(3-hydroxybutyrate) plasticized with acetyl tributyl citrate, Polym. Degrad. Stab. 90 (2) (2005) 313–318.
[84] K.L. Dagnon, H.H. Chen, L.H. Lnnocentini-Mei, N.A. D'Souza, Poly (3-hydroxybutyrate)-co-(3-hydroxyvalerate)/layered double hydroxide nanocomposites, Polym. Int. 58 (2) (2009) 133–141.
[85] S. Torres-Giner, N. Montanes, O. Fenollar, D. García-Sanoguera, R. Balart, Development and optimization of renewable vinyl plastisol/wood flour composites exposed to ultraviolet radiation, Mater. Des. 108 (2016) 648–658.
[86] S. Torres-Giner, A. Chiva-Flor, J.L. Feijoo, Injection-molded parts of polypropylene/multi-wall carbon nanotubes composites with an electrically conductive tridimensional network, Polym. Compos. 37 (2) (2016) 488–496.